Fractal-Based Ensemble Classification System for Hyperspectral Images

Article *in* IEEE Geoscience and Remote Sensing Letters · November 2023

DOI: 10.1109/LGRS.2023.3330608

3 authors:

Behnam Asghari Beirami
Khaje Nasir Toosi University of Technology
34 PUBLICATIONS **159** CITATIONS
SEE PROFILE

Mehran Alizadeh Pirbasti
University College Dublin
4 PUBLICATIONS **1** CITATION
SEE PROFILE

Vahid Akbari
University of Stirling
58 PUBLICATIONS **666** CITATIONS
SEE PROFILE

Fractal-based Ensemble Classification System for Hyperspectral Images

Behnam Asghari Beirami, Mehran A Pirbasti, and Vahid Akbari, *Member, IEEE*

***Abstract*—According to the literature, the utilization of spatial features can significantly enhance the accuracy of hyperspectral image (HSI) classification. Fractal features are powerful measures of texture, representing the local complexity of an image. In HSI classification, textural features are typically extracted from dimensionally reduced datacubes, such as principal component analysis (PCA). However, the effectiveness of textures obtained from alternative feature extraction methods in improving classification accuracy has not been extensively investigated. This study introduces a new ensemble support vector machine classification system that combines spectral features derived from PCA, minimum noise fraction, linear discriminant analysis, and fractal features derived from these feature extraction methods. The final results on two HSI datasets, namely Indian Pines and Pavia University, demonstrate that the proposed classification method achieves approximately 95.75% and 99.36% accuracies, outperforming several other spatial-spectral HSI classification methods.**

***Index Terms*—Ensemble learning, Hyperspectral image, Fractal dimension, Voting-based fusion**

I. Introduction

HYPERSPECTRAL images (HSI) are three-dimensional datasets captured using hyperspectral sensors mounted on airborne or spaceborne platforms. These images provide detailed spectral information about surface materials across different wavelengths of electromagnetic waves [1], enabling the differentiation of various ground classes. However, the classification of these large and complex datasets can be challenging, particularly in cases where training samples are limited [1].

One major issue associated with the high dimensionality of HSI is known as "the curse of dimensionality", which can lead to reduced classifier performance [2]. Additionally, within-class spectral variability and between-class spectral similarity reduce spectral-based classification accuracy, leading to noisy classified images. [1]. To tackle these challenges, researchers have proposed feature extraction (FE) methods to address high dimensionality in HSIs [3], [4]. FE methods can be categorized as supervised or unsupervised. Unsupervised techniques, such as Principal Component Analysis (PCA), transform features into a new uncorrelated space known as principal components [5]. Minimum Noise Fraction (MNF) is another unsupervised method that reduces noise and organizes features based on their signal-to-noise ratio (SNR) [6]. In contrast, supervised techniques like Linear Discriminant Analysis (LDA) utilize training samples to construct a transformation matrix. LDA uses within-class and between-class scatter matrices to project features into a discriminative space [7].

In addition to spectral information, the spatial information of pixels within HSIs serves as another valuable data source that can address within-class spectral variability and between-class similarities in the spectral behavior of materials, ultimately improving classification accuracy. Different methods exist for generating spatial features, each capturing contextual information from unique perspectives [8], [9]. Morphological Profiles (MPs), based on the opening and closing morphological operators, are widely used spatial features for HSI classification. Beirami and Mokhtarzade introduced an HSI classification method that initially employs MPs classified with Support Vector Machines (SVM), followed by post-processing using the guided filter [10]. Extinction profiles are another spatial feature employed by Kakhani et al. in combination with deep learning models for remote sensing image classification [11]. In addition to geometric features, textural features like Gabor filters are extensively used in various studies to accurately classify HSIs in different directions and orientations [1], [12]. For further information regarding the various spatial feature generation methods, please refer to [8].

Utilizing Fractal Dimension (FD) is an effective method for generating spatial features. FD quantifies the complexity of fractal patterns and is considered a key feature [13]. For grayscale images, the numerical value of FD typically falls within the range of two and three, depending on image complexity [13]. In Zhu et al.'s study, a combination of FD features and spectral bands of Landsat ETM+ images were employed to classify mountainous areas in China [14]. Similarly, Mehdi and Hassan incorporated FD features in their research for the supervised classification of high-resolution QuickBird images [15], demonstrating the accurate discrimination of classes in satellite images. Within the domain of HSI classification, Beirami and Mokhtarzade integrated multiple fractal features with spectral features to enhance the accuracy of image classification [16]. Their research suggests that fractal features possess significant potential to improve the classification accuracy of HSIs. Spatial features in HSI classification are often derived from reduced-dimension images to overcome computational challenges. These images, obtained through various FE methods, exhibit distinct textures for different classes. Utilizing textural information from diverse reduced images

Manuscript received xxx; 2023; revised xxx, 2024; accepted xxx, 2024. Date of publication xxx, 2024;

B. A. Beirami is with the Department of Photogrammetry and Remote Sensing, Faculty of Geodesy and Geomatics, K. N. Toosi University of Technology, Tehran, Iran, behnam.asghari1370@gmail.com.

M. A. Pirbasti is with the SFI Centre for Research Training in Machine Learning at School of Computer Science, University College Dublin, Ireland. mehran.alizadehpirbasti@ucdconnect.ie.

V. Akbari is with the Division of Computing Science and Mathematics, University of Stirling, Stirling, FK9 4LA, UK. vahid.akbari@stir.ac.uk.

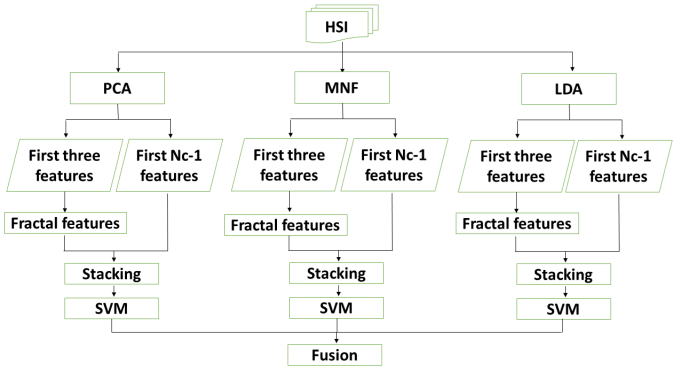

Fig. 1. Flowchart of the proposed method

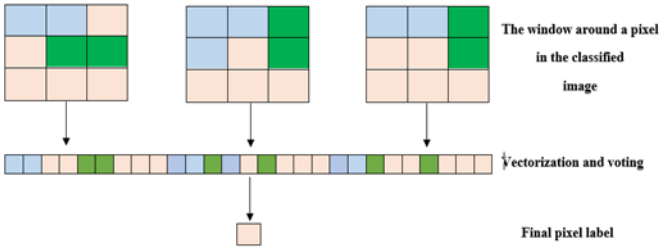

Fig. 2. IVF method

created with different FE methods can improve classification accuracy. Motivated by the effectiveness of fractal features in remote sensing image classification, we propose a novel ensemble HSI classification system. This system combines spectral and fractal features generated from different FE methods, contributing to improved HSI classification performance, addressing challenges, and achieving accurate results with limited training samples.

The subsequent section provides a detailed explanation of our proposed method, including feature extraction techniques, fractal dimension, and the voting method. In Section III, we analyze the accuracy results of our method and compare them with other existing HSI classification methods. Finally, in Section IV, we present our concluding remarks for this study.

II. METHODOLOGY

Fig.1 illustrates the flowchart of the proposed ensemble approach, comprising five main stages outlined below:

1) The HSI image undergoes dimensionality reduction using three feature extraction methods: PCA, MNF, and LDA.

2) fractal features are generated from the first three components of each dimensionality-reduced feature cube.

3) The reduced spectral data cube with Nc-1 bands (where Nc represents the number of classes) and its fractal features are combined through stacking.

4) Each branch is classified using an SVM classifier with kernel strategy, resulting in label maps.

5) The classification results from all three branches are fused using an improved voting fusion (IVF) method.

Further information about each stage is provided in the subsequent subsections.

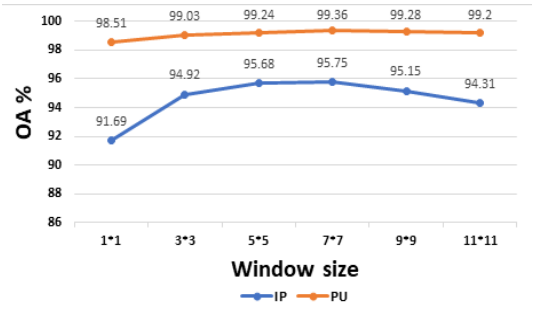

Fig. 3. Impact of window size on the performance of IVF method

A. Feature extraction methods

In this study, we utilize three widely used FE methods, namely PCA, MNF, and LDA, to extract the informative low-dimensional spectral features. More detailed information on these methods can be found in the references [5]–[7], while a brief summary is presented below.

• PCA is a commonly employed method for reducing dimensional complexity in data. This unsupervised technique aims to transform a set of correlated variables into a smaller number of uncorrelated variables called principal components. These components represent the directions of maximum variance within the data and are orthogonal to one another.

• MNF is an unsupervised feature extraction technique specifically developed for hyperspectral imagery. This method utilizes the covariance matrix of both data and noise to transform the input data into a new feature space. Unlike PCA, MNF ranks extracted features based on their signal-to-noise ratio (SNR) rather than variance. As a result, MNF may be more effective in reducing noise while preserving spectral information.

• LDA is a supervised technique for reducing dimensionality that identifies the optimal projection of a training dataset to best separate examples according to their assigned class. LDA employs class labels to determine the directions that maximize the separation between classes. Utilizing LDA can potentially improve classification accuracy, reduce overfitting, and facilitate clearer data visualization.

B. Fractal features

Fractal dimension (FD) as a textural measure is commonly obtained using the Pentland method [17], which follows a directional approach. This method takes into account spectral variations in the neighboring region of each pixel to extract fractal features. The self-similarity parameter (H) is defined based on the difference in grey level between two pixels at a distance r denoted by E_r and a constant value denoted as E_0 by [16]:

$$E_r r^{-H} = E_0. \tag{1}$$

The FD is then calculated using the following [16]:

$$FD = 1 - H. \tag{2}$$

TABLE I
CLASSIFICATION ACCURACIES FOR THE IP IMAGE, INCLUDING OVERALL ACCURACY (OA), THE KAPPA COEFFICIENT, Z INDEX.

Class #	SVM-Spectral	SVM-PCA	SVM-MNF	SVM-LDA	PCA-Fractal	MNF-Fractal	LDA-Fractal	**Proposed method**
1	20.93%	69.76%	86.04%	20.93%	83.72%	**100%**	90.69%	97.67%
2	68.16%	58.87%	80.91%	51.28%	81.80%	89.38%	75.97%	**90.56%**
3	55.76%	63.62%	70.97%	59.56%	90.24%	93.53%	86.43%	**99.11%**
4	45.13%	27.87%	51.76%	37.16%	75.66%	77.87%	69.91%	**80.08%**
5	85.18%	87.36%	96.73%	71.45%	91.72%	**97.16%**	91.28%	95.42%
6	93.08%	92.36%	98.41%	87.03%	98.70%	97.26%	97.55%	**99.27%**
7	80.00%	64.00%	100%	68.00%	100%	100%	100%	**100%**
8	96.92%	96.26%	93.84%	94.50%	98.24%	100%	98.46%	**100%**
9	35.29%	35.29%	100%	41.17%	100%	100%	100%	**100%**
10	56.06%	39.93%	71.53%	51.19%	79.97%	89.17%	80.41%	**92.74%**
11	74.71%	64.59%	72.82%	69.09%	85.51%	93.14%	87.01%	**97.17%**
12	60.99%	42.02%	79.96%	52.12%	69.14%	88.29%	76.77%	**91.84%**
13	98.46%	94.87%	**99.48%**	89.74%	91.79%	96.41%	94.87%	92.30%
14	88.51%	79.28%	90.68%	82.61%	99.25%	96.58%	98.16%	**99.91%**
15	50.13%	42.50%	70.29%	42.50%	95.36%	91.00%	86.10%	**99.72%**
16	86.51%	80.89%	92.13%	84.26%	**97.75%**	86.51%	86.51%	88.76%
OA	72.92%	65.45%	80.53%	65.95%	87.86%	92.85%	86.86%	**95.75%**
Kappa	0.684	0.60	0.774	0.60	0.86	0.917	0.847	**0.95**
$\|Z - index\|$	23.7	29.46	15.3	30.03	7.94	2.19	8.68	**reference**

TABLE II
CLASSIFICATION ACCURACIES FOR THE PU IMAGE, INCLUDING OVERALL ACCURACY (OA), THE KAPPA COEFFICIENT, Z INDEX.

Class #	SVM-Spectral	SVM-PCA	SVM-MNF	SVM-LDA	PCA-Fractal	MNF-Fractal	LDA-Fractal	**Proposed method**
1	91.19%	88.52%	89.36%	89.34%	97.84%	97.23%	95.92%	**99.74%**
2	95.33%	94.62%	96.68%	95.00%	99.04%	98.37%	99.01%	**99.69%**
3	75.58%	72.93%	69.07%	72.48%	94.43%	97.34%	92.23%	**99.79%**
4	92.16%	90.41%	92.57%	85.54%	99.00%	98.48%	99.14%	98.66%
5	99.37%	99.37%	99.84%	99.53%	100%	100%	100%	**100%**
6	82.54%	67.78%	86.47%	75.09%	99.12%	97.06%	99.22%	**99.85%**
7	73.57%	83.93%	82.99%	82.51%	92.24%	92.32%	86.15%	**97.54%**
8	80.73%	80.07%	80.61%	82.33%	95.59%	95.14%	94.59%	**98.51%**
9	**99.88%**	**99.88%**	99.44%	99.88%	91.77%	92.66%	94.44%	93.88%
OA	90.28%	87.83%	91.05%	88.77%	97.99%	97.46V	97.38%	**99.36%**
Kappa	0.87	0.836	0.88	0.849	0.973	0.966	0.965	**0.991**
$\|Z - index\|$	13.76	19.46	13.18	16.73	2.82	3.32	3.95	**reference**

By taking the logarithm of both sides of eq.(1), we obtain the following [16]:

$$\log(E_r) - H\log(r) = C_0 \tag{3}$$

The values of H and C_0 can be determined by fitting a linear regression line between $\log(E_r)$ and $\log(r)$, where H represents the slope and C_0 denotes the intercept [16]. Interestingly, C_0 represents a new fractal feature called "intersection" [16]. In this study, we utilize a combination of fractal dimension and intersection features as fractal features.

To extract fractal features using the Pentland method, each pixel is initially surrounded by a moving window of size L. Then, a random variable r is selected in a specific direction within the range of $(0, L)$, where r represents the difference between two random variables a and b, satisfying the condition $0 < a < b \leq L$. Subsequently, the parameter e_r is computed as [16]:

$$e_r = \frac{|S_b - S_a|}{r+1}, \tag{4}$$

where S_b and S_a correspond to the grey values of pixels at distances r and in the assumed direction. Given the positive integer a, the average of the parameter e_r can be calculated as follows [16]:

$$\bar{e}_r = \frac{\sum_{a=0}^{L-r} e_r}{L-r+1}. \tag{5}$$

E_r is then given as [16]:

$$E_r = \bar{e}_r \frac{L}{r} \tag{6}$$

The Pentland method calculates the fractal features using a directional approach, considering four directions: north, south, northwest to southeast, and northeast to southwest. This results in different values of H and C_0 for each direction. In this study, fractal features are generated with window sizes of 9×9, 17×17, and 25×25 to capture the spatial characteristics of objects with different sizes more effectively.

C. Improved voting fusion

Based on Fig. 1, we employed various feature extraction methods to extract fractal features, and subsequently utilized SVM for the classification of the stacked spatial and spectral features. Next, we fused the three classified images to generate the final classification image, adopting an improved voting fusion method inspired by [18]. In traditional voting fusion, the most frequent label from classified images for each pixel

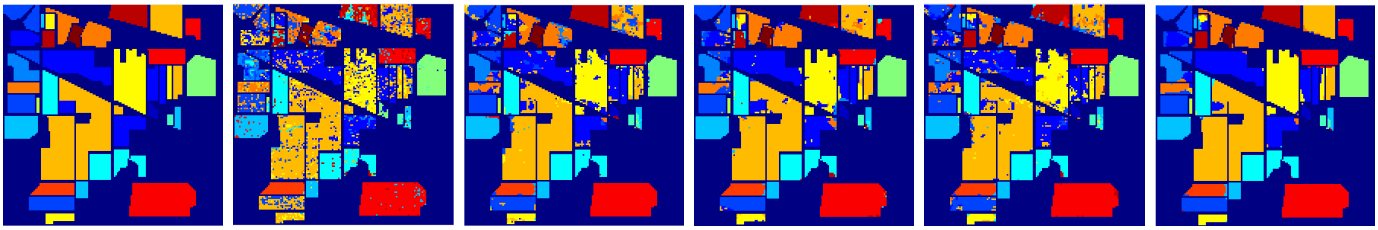

(a) (b) (c) (d) (e) (f)

Fig. 4. Classification maps of IP dataset a) GT image, b) SVM-spectral, c) PCA-Fractal, d) MNF-Fractal, e) LDA-Fractal, f) Proposed method.

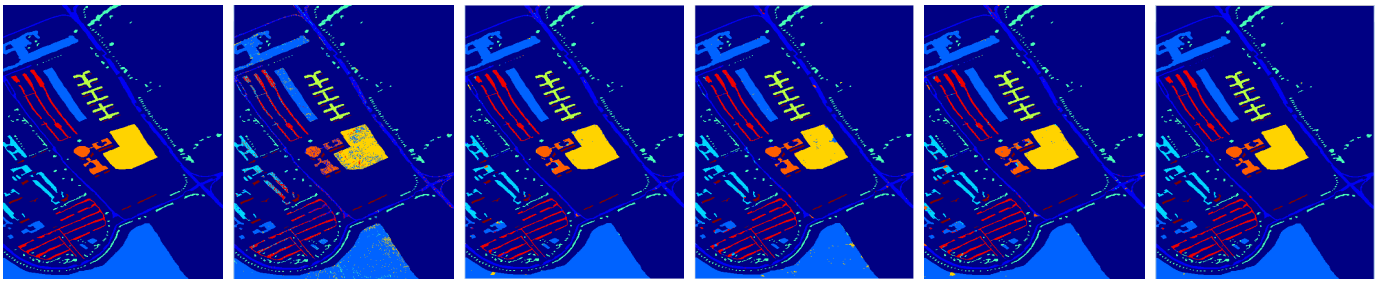

(a) (b) (c) (d) (e) (f)

Fig. 5. Classification maps of PU dataset a) GT image, b) SVM-spectral, c) PCA-Fractal, d) MNF-Fractal, e) LDA-Fractal, f) Proposed method.

determines the final label, but this can lead to noisy results. To overcome this, the IVF method is applied, which considers neighboring information. The IVF method involves three steps Fig.2: defining a window around each pixel, reshaping the labels within the window into a vector, and selecting the most frequent label from the combined vectors as the label for the center pixel. The IVF method produces smoother transitions compared to the conventional voting method by incorporating neighboring information. The traditional voting technique can be seen as a specific case of IVF, where the window size is reduced to a single pixel, considering only the center pixel.

III. DATASET AND EXPERIMENTAL RESULTS

A. Dataset

In this research, we utilized two well-known hyperspectral images, with the following descriptions: Indian Pines (IP): The IP dataset is a widely recognized HSI benchmark collected by the AVIRIS hyperspectral sensor in Indiana, USA. It contains 145x145 pixels, with 200 spectral bands after excluding low-information bands. The dataset includes 16 different classes, including crops and semi-urban features.

Pavia University (PU): The PU dataset is an aerial HSI captured by the ROSIS sensor. It comprises 115 spectral bands, with a spatial resolution of 1.3 meters and dimensions of 610×340 pixels. After excluding 12 bands with low information content, a total of 103 bands were utilized in the experiments.

B. Experimental results

In subsequent experiments, 5% of pixels from each class were randomly selected for training, while the rest were used for testing classification accuracy. Evaluation metrics included OA, kappa coefficient, and class accuracies. MATLAB 2020b was used on a system with a core i5 4090 CPU and 8GB DDR3 RAM.

The first experiment focused on window size's impact on IVF classification accuracy. Window sizes ranged from 1x1 to 11x11 with a step size of 2. Results showed that 7x7 was the optimal window size for IVF, with accuracy improving up to that point and decreasing afterward (Fig.3). Larger window sizes considered more surrounding pixels, which could compromise IVF performance, particularly at class edges and for small classes.

In our second experiment, we compared our spatial-spectral ensemble strategy to two groups of techniques: spectral-based HSI classification methods and individual branches of our method. The spectral-based methods included SVM-original Spectral, SVM-PCA, SVM-MNF, and SVM-LDA, while the individual branches were PCA-Fractal, MNF-Fractal, and LDA-Fractal followed by SVM classification. Our ensemble approach demonstrated effectiveness, as shown by the classification accuracy in Tables I and II for IP and PU datasets. Solely using spectral features with SVM did not yield high accuracy, but integrating spatial fractal features improved classification results for both datasets. Combining the classification results of each branch in our proposed method significantly increased accuracy, as confirmed by the Z-score results (all values exceeding 1.96) [1]. Fig.4 and Fig.5 show the ground truth (GT) and final classification images, indicating a significant decrease in misclassified pixels compared to alternative methods.

In the final experiment of this section, we conducted a comparison between our proposed method and five other spatial-spectral HSI classification methods proposed in previous studies [9], [19]–[22]. Mirzapour *et al.* [9] utilized

TABLE III
COMPARISON WITH OTHER METHODS

	IP	*PU*
Method	***OA***	
Mirzapour*et al.* [9]	92.78%	98.95%
Majdar*et al.* [19]	95.07%	98.21%
Wang*et al.* [20]	—*	98.52%
Ghaderizadeh*et al.* [21]	93.27%	—*
Cai*et al.* [22]	77.61%	95.24%
Proposed Method	**95.75**%	**99.36**%

* The result is not reported in the original paper

spectral and spatial features, such as MPs, Gabor, and gray-level co-occurrence matrices, along with an SVM classifier. Majdar *et al.* [19] introduced a three-step approach that combines probabilistic SVM results from spectral and Gabor features. Wang *et al.* [20] improved the performance of low-rank representation by incorporating locality constraint criteria and a structure-preserving strategy. Ghaderizadeh *et al.* [21] employed a 3D fast learning block and a 2D CNN to extract spectral-spatial features. Cai *et al.* [22] proposed a new triple-attention mechanism to assign weights to diverse features. It utilized a residual network to perform residual operations and merge these features with deep residual features using multiple blocks. The contextual semantics of the deep fusion features were integrated using a BiLSTM network, and classification was performed using a softmax classifier. Classification accuracies of various methods are reported in Table III. Our proposed ensemble fractal classification method demonstrated superior performance compared to other spatial-spectral classification methods.

The proposed ensemble method has a processing time of around 260 seconds on the IP dataset. This processing time is better than competitor methods like Wang *et al.* and Majdar *et al.*, which require approximately 336 and 580 seconds respectively. It is important to mention that parallel computing can further reduce implementation time. In this approach, each branch of the ensemble system is implemented on a separate system, and the results are combined afterward.

IV. CONCLUSIONS

We propose an ensemble system using three SVM classifier branches (PCA, MNF, and LDA) with fractal features for HSI classification. Results on Indian Pines and Pavia University datasets show a significant accuracy improvement of 22% and 9%, respectively. The three-branch strategy outperforms individual branches by 6.5% and 1.75% on average. Our method is efficient and surpasses other classification methods. Future work aims to enhance performance with advanced classifiers and post-processing techniques.

REFERENCES

[1] B. A. Beirami and M. Mokhtarzade, "Hyperspectral image classification using multiple weighted local kernel matrix descriptors," *International Journal of Remote Sensing*, vol. 43, no. 14, pp. 5280–5305, 2022.

[2] S. H. A. Moghaddam, M. Mokhtarzade, and B. A. Beirami, "A feature extraction method based on spectral segmentation and integration of hyperspectral images," *International Journal of Applied Earth Observation and Geoinformation*, vol. 89, p. 102097, 2020.

[3] J. Khodr and R. Younes, "Dimensionality reduction on hyperspectral images: A comparative review based on artificial datas," in *2011 4th international congress on image and signal processing*, vol. 4. IEEE, 2011, pp. 1875–1883.

[4] B. Rasti, D. Hong, R. Hang, P. Ghamisi, X. Kang, J. Chanussot, and J. A. Benediktsson, "Feature extraction for hyperspectral imagery: The evolution from shallow to deep: Overview and toolbox," *IEEE Geoscience and Remote Sensing Magazine*, vol. 8, no. 4, pp. 60–88, 2020.

[5] M. A. M. Md. Palash Uddin and M. A. Hossain, "Pca-based feature reduction for hyperspectral remote sensing image classification," *IETE Technical Review*, vol. 38, no. 4, pp. 377–396, 2021.

[6] L. Fang, N. He, S. Li, A. J. Plaza, and J. Plaza, "A new spatial–spectral feature extraction method for hyperspectral images using local covariance matrix representation," *IEEE Transactions on Geoscience and Remote Sensing*, vol. 56, no. 6, pp. 3534–3546, 2018.

[7] S. D. Fabiyi, P. Murray, J. Zabalza, and J. Ren, "Folded LDA: Extending the linear discriminant analysis algorithm for feature extraction and data reduction in hyperspectral remote sensing," *IEEE Journal of Selected Topics in Applied Earth Observations and Remote Sensing*, vol. 14, pp. 12 312–12 331, 2021.

[8] B. Kumar, O. Dikshit, A. Gupta, and M. K. Singh, "Feature extraction for hyperspectral image classification: A review," *International Journal of Remote Sensing*, vol. 41, no. 16, pp. 6248–6287, 2020. [Online]. Available: https://doi.org/10.1080/01431161.2020.1736732

[9] F. Mirzapour and H. Ghassemian, "Improving hyperspectral image classification by combining spectral, texture, and shape features," *International Journal of Remote Sensing*, vol. 36, no. 4, pp. 1070–1096, 2015.

[10] B. A. Beirami and M. Mokhtarzade, "Spatial-spectral classification of hyperspectral images based on extended morphological profiles and guided filter," *Computer and Knowledge Engineering*, vol. 2, no. 2, pp. 2–8, 2020.

[11] N. Kakhani, M. Mokhtarzade, and M. J. Valadan Zoej, "Deep learning spatial-spectral classification of remote sensing images by applying morphology-based differential extinction profile (dep)," *Electronics*, vol. 10, no. 23, p. 2893, 2021.

[12] S. Jia, Z. Lin, B. Deng, J. Zhu, and Q. Li, "Cascade superpixel regularized gabor feature fusion for hyperspectral image classification," *IEEE transactions on neural networks and learning systems*, vol. 31, no. 5, pp. 1638–1652, 2019.

[13] W. Sun, G. Xu, P. Gong, and S. Liang, "Fractal analysis of remotely sensed images: A review of methods and applications," *International Journal of remote sensing*, vol. 27, no. 22, pp. 4963–4990, 2006.

[14] J. Zhu, J. Shi, H. Chu, J. Hu, X. Li, and W. Li, "Remote sensing classification using fractal dimensions over a subtropical hilly region," *Photogrammetric Engineering & Remote Sensing*, vol. 77, no. 1, pp. 65–74, 2011.

[15] M. S. Mahdi and A. A. A. Hassan, "Satellite images classification in rural areas based on fractal dimension," *Journal of Engineering*, vol. 22, no. 4, pp. 147–157, 2016.

[16] B. A. Beirami and M. Mokhtarzade, "Spatial-spectral classification of hyperspectral images based on multiple fractal-based features," *Geocarto International*, vol. 37, no. 1, pp. 231–245, 2022.

[17] A. P. Pentland, "Fractal-based description of natural scenes," *IEEE transactions on pattern analysis and machine intelligence*, no. 6, pp. 661–674, 1984.

[18] Z. Lv, X. Zhang, and J. A. Benediktsson, "Developing a general post-classification framework for land-cover mapping improvement using high-spatial-resolution remote sensing imagery," *Remote Sensing Letters*, vol. 8, no. 7, pp. 607–616, 2017.

[19] R. Seifi Majdar and H. Ghassemian, "A probabilistic SVM approach for hyperspectral image classification using spectral and texture features," *International Journal of Remote Sensing*, vol. 38, no. 15, pp. 4265–4284, 2017.

[20] Q. Wang, X. He, and X. Li, "Locality and structure regularized low rank representation for hyperspectral image classification," *IEEE Transactions on Geoscience and Remote Sensing*, vol. 57, no. 2, pp. 911–923, 2018.

[21] S. Ghaderizadeh, D. Abbasi-Moghadam, A. Sharifi, N. Zhao, and A. Tariq, "Hyperspectral image classification using a hybrid 3d-2d convolutional neural networks," *IEEE Journal of Selected Topics in Applied Earth Observations and Remote Sensing*, vol. 14, pp. 7570–7588, 2021.

[22] W. Cai, B. Liu, Z. Wei, M. Li, and J. Kan, "TARDB-net: triple-attention guided residual dense and bilstm networks for hyperspectral image classification," *Multimedia Tools and Applications*, vol. 80, pp. 11 291–11 312, 2021.